

Research Article

A Multi Response Optimization of Tool Pin Profile on the Tensile Behavior of Age-hardenable Aluminum Alloys during Friction Stir Welding

¹D. Vijayan and ²V. Seshagiri Rao

¹Department of Mechanical Engineering, Sri Chandrasekharendra Saraswathi Viswa Maha Vidyalaya, Enathur, Kanchipuram-631561, Tamilnadu, India

²St. Josephs College of Engineering, Chennai-600025, Tamilnadu, India

Abstract: The main aim of this study is to select a suitable tool pin profile to maximize the tensile behavior (Ultimate Tensile Strength and Tensile Elongation) of Friction stir welded aluminum alloys of AA 2024 and AA 6061. The age-hardenable aluminum alloys of 2xxx, 6xxx and 7xxx series are extensively used in automobile and aircraft industries because of its high strength to weight ratio, formability and ductility. These alloys are vulnerable to cracking (2xxx and 7xxx) and highly melt (6xxx) in conventional fusion welding techniques. Friction stir welding is an emerging solid state welding technique which is best suitable for joining these aluminum alloys. The influential process and tool parameters that are affecting the FS welded joints are such as tool rotational speed, welding speed, axial load and tool pin profile. Dissimilar friction stir welded joints of AA 2024 and AA 6061 aluminum alloys are fabricated using a friction stir welding process to examine the influence of the tool pin profiles on tensile properties on various crucial process parameters. A Box-Behnken design with four input parameters, three levels and 30 runs is used to conduct the experiments and Response Surface Method (RSM) is used to develop the mathematical model. The experimental results were predicted at the 95% confidence level. The macro defects in the welds and the modes of tensile fracture are discussed in detail to reveal the root cause of failure in the fabricated samples. The rotating tool equipped with a square pin generated the highest ultimate tensile strength (143 MPa) with a 12% elongation. A microstructure variation on dissimilar alloys which result 44% reduction in tensile strength on AA2024 and 51% reduction in tensile strength on AA6061 aluminum alloys was observed on the stir zones.

Keywords: Aluminum, desirability, elongation, friction stir welding, optimization, response surface, tensile

INTRODUCTION

The conventional fusion welding techniques such as arc, gas welding of age hardenable aluminum alloys (2xxx, 6xxx and 7xxx) are a challenging task for designers and technologists. Since, the difficulties in the fusion welding process are associated mainly related to the presence of the oxide layer, solidification shrinkage, high coefficient of thermal expansion, high thermal conductivity and other gases in a molten state (Shanmuga Sundaram and Murugan, 2010). Joining these alloys using fusion welding techniques leads to the melting and re-solidification of the fusion zone, results the formation of brittle inter-dendritic structure and eutectic phases. The formation of brittle structure in the weld zone results a drastic loss of mechanical properties (Rhodes *et al.*, 1997; Su *et al.*, 2003). Generally, aluminum alloys of AA 2024 (Al-Cu alloy) extensively used for aerospace applications because of its high strength to weight ratio however these alloys are classified into non weldable since these alloys are sensitive to cracking (Shanmuga Sundaram and

Murugan, 2010) due to its copper alloying element. The heat provided in fusion welding decay the mechanical properties lead phase transformation and softening the fusion zone is significant. Few 2xxx grades of aluminum alloys can be resistance welded but surface preparation is expensive. Aluminum alloys of AA 6061 (Al-Mg-Si) are mainly used for commercial applications of marine and automotive fittings, bicycle frames etc. These AA 6061 aluminum alloys can be welded using TIG, MIG welding however, losses of mechanical properties near the fusion zone are significant. Therefore, fusion welding techniques are not suitable for the dissimilar welding of aluminum alloys AA 2024 and AA 6061, therefore friction stir welding process could be the best for the dissimilar welding of these alloys.

Friction Stir Welding (FSW) was invented in December 1991 by Wayne Thomas and a team of his colleagues at The Welding Institute UK (Thomas *et al.*, 1991; Dawes and Thomas, 1995). It is an innovative and emerging technique in the solid state welding. A non consumable steel tool rotates around its axis to the

Corresponding Author: D. Vijayan, Department of Mechanical Engineering, Sri Chandrasekharendra Saraswathi Viswa Maha Vidyalaya, Enathur, Kanchipuram-631561, Tamilnadu, India

This work is licensed under a Creative Commons Attribution 4.0 International License (URL: <http://creativecommons.org/licenses/by/4.0/>).

abutting edge of the plates and the heat is generated as a result of the contact between the surfaces of the tool and work piece. Compared to other welding techniques, FSW offers many advantages, such as low residual stresses, little distortion; high joint strength and bulk melting are avoided (Dawes and Thomas, 1995). Friction stir welding immune defects and deteriorations associated with the fusion welding are limited. Addition to that, the extensive thermo mechanical deformation induces dynamic re-crystallization that refines the micro structure on FS welded region therefore mechanical properties are improved such tensile strength, hardness etc.

Numerous numbers of studies have been performed and imparted significance of dissimilar joining of aluminum alloys of friction stir welding. Hu *et al.* (2012) investigated the tensile deformation characteristics of AA 2024 aluminum alloys. It is reported that, the FS welded joint has diverse characteristics on tensile deformation leading significant reduction in global ductility. Mohammadtaheri *et al.* (2013) investigated the effects of base material conditions on the friction stir welding of AA 2024 aluminum alloys. It was found that, the average grain sizes of base material and stirred zone are almost identical. Da Silva *et al.* (2011) evaluated the joining parameters of AA 2024 aluminum alloys using friction stir welding to understand the mixing process and identified no material mixing was attained however a fine grained stirred zone was observed on the micro structural observation. Ying *et al.* (2000) reported in their study on friction stir welding of AA 2024 to silver. It is reported, the age hardenable aluminum alloys (2xxx, 6xxx, 7xxx series) are suffer strength degradation due to microstructure variation during mixing especially, in the narrow regime just outside the FSW zone. Ouyang and Kovacevic (2002) investigated the material flow and microstructure in the friction stir welded butt joints of same and dissimilar aluminum alloys of AA 6061 and AA 2024. It is reported in this study, there is a substantial variation in hardness throughout the nugget zone. Addition to that, the degree of mixing, material flow patterns are associated with the process parameters. Therefore, suitable parameters are supposed to provide to obtain a significant joint strength of the weld joints. The important process and tool parameters that are affecting the joint strength of FS welded joints are rotational speed (N), the welding speed (F) axial load (P) and pin profiles such as cylindrical, square, tapered and hexagonal. These parameters are vital for the material flow pattern, the mechanical and metallurgical transformation and the temperature distribution of the weld joints. The effects of the tool pin have been investigated by varying the tool pin profile on various aluminum and its alloys (Kwon *et al.*, 2012; Dehghani *et al.*, 2013). In those

investigations are demonstrated using mathematical and statistical approaches. The mathematical approaches that are commonly used to select the process parameters are time consuming, requiring extensive resources to obtain a feasible solution (Lakshminarayanan and Balasubramanian, 2008). Therefore, these types of complex problems can be solved using statistical techniques. Especially when the responses have diversity then the multi objective optimization techniques are applied. Sefika (2013) used taguchi based grey relational analysis to improve the ultimate tensile strength and elongation of friction stir welded AA6082-T6/AA5754-H111 aluminum alloys. Elmesalamy *et al.* (2013) used response surface methodology to understand the process parameter selection for laser welding process. Muhammad *et al.* (2013) used Taguchi based response surface methodology to develop the quality features of resistance spot welding technique. Anish *et al.* (2013) applied response surface methodology for setting the optimal input process parameters for the WEDM process. Exclusively, in friction stir welding; Rajakumar and Balasubramanian (2012) used desirability approach to optimize the AA1100 aluminum alloy using friction stir welding technique, Lakshminarayanan and Balasubramanian (2008) used response surface technique to optimize the process parameters of AA7039 aluminum alloy joints, Karthikeyan and Balasubramanian (2010) predicted optimized welding parameters for joining AA2024 aluminum alloy using response surface methodology. Therefore, numerous investigations reveal the various statistical methodologies for obtaining the suitable parameter selection when the diversified objective; however, those investigations are not discussing about dissimilar FS welding of AA2024 and AA6061 aluminum alloys. Hence, in this present investigation, a multi response optimization approach called response surface method using desirability function is applied in order to maximize the ultimate tensile strength and tensile elongation of age hardenable aluminum alloys of AA6061-AA2024.

Experimental setup: A home-built FSW machine was used to fabricate the weld joints. A schematic arrangement for the aluminum alloy plate during the welding process is shown in Fig. 1. AA2024-T3 and AA6061-T6 aluminum alloys are selected for the dissimilar FS welding process. T3 represents the AA2024 alloy, which is solution heat-treated, cold-worked and naturally aged to a substantially stable condition. To improve strength, the alloy was subjected to a solution heat treatment for which the mechanical properties were stabilized during room-temperature aging. T6 denotes AA6061 alloys that are solution heat-treated and artificially aged. These products are not



Fig. 1: FSW machine setup and position of aluminum alloys

Table 1: Chemical composition and mechanical properties of AA2024 and AA6061 aluminum alloy

Aluminum alloy (%)	Cr	Cu	Fe	Mg	Mn	Si	Tensile yield strength (MPa)	Elongation (%)
2024	0.10	4.90	0.90	1.80	0.90	0.50	324	20
6061	0.35	0.40	0.70	1.20	0.15	0.80	276	17

Table 2: Process parameters and their range

Process parameters	Unit	Range		
		-1	0	1
Rotational speed	rpm	1500	1700	1900
Welding speed	mm/min	30	60	90
Axial load	kN	3	6	9
Pin shape		1 (tap)	2 (Squ)	3 (Cyl)

cold worked after the solution heat treatment (ASM Handbook, 1990). The mechanical and chemical compositions of each alloy are presented in Table 1. Aluminum alloys as 300×150×6.25 mm, respectively plates are used to fabricate the butt joint. The tool rotates perpendicular to the longitudinal surface of the plate. When the tool rotation and translation of the plate movement occur in the same direction, the plate position is referred as the retreating side. When the rotation and translation are opposed, the plate position is referred as the advancing side. When the rotation and translation are opposed, the plate position is referred as the advancing side. Since, the weld nugget predominantly occupies the retreating side metal (Lee *et al.*, 2003). Therefore, a high strength aluminum alloy (AA2024-T3) is placed on the retreating side, while a low strength aluminum alloy (AA6061-T6) is placed on the advancing side of the FS weld joint. Based on a thorough literature investigation, the parameters used in the present study, such as the tool rotational speed (N), welding speed (F), axial force (P) and pin profiles, are selected (Biswas *et al.*, 2012; Kalaiselvan and

Murugan, 2013; Jayaraman and Balasubramanian, 2013). Three major pin profiles are assessed in the present study: Taper (TA), Square (SQ) and Straight Cylinder (SC). SKD -61 tool steel is used to fabricate the rotating tools. This metal is a chromium-molybdenum hot-worked air-hardening steel and therefore has good wear resistance, elevated-temperature strength and thermal fatigue resistance (Lomolino *et al.*, 2005). The fabricated FSW tools are shown in Fig. 2. The process parameters and their values are presented in Table 2. The fabricated weld samples are kept for further mechanical and metallurgical characterization. The test pieces were prepared from the welded samples to estimate the joint strength and undertake metallographic examinations. The tensile specimens were cut perpendicular to their rolled direction. The test was conducted as per the American Standard for Testing of Materials (ASTM) standard IX reference; the dimensions and fracture samples are in presented in Fig. 3. The design matrix, including the recorded experimental values for the ultimate tensile strength and tensile elongation, is



Fig. 2: Fabricated FSW tools

Table 3: Design matrix with their experimental values of Ultimate Tensile Strength (UTS), Tensile Elongation (TE)

Exp No.	Rotational speed (rpm)	Welding speed (mm/min)	Axial load (kN)	Pin shape	Ultimate tensile strength (Mpa)	Tensile elongation (%)
1	1500	30	6	2	108.31	10.64
2	1900	30	6	2	109.33	9.12
3	1500	90	6	2	109.32	11.64
4	1900	90	6	2	101.06	9.62
5	1700	60	3	1	122.25	12.64
6	1700	60	9	1	127.09	9.64
7	1700	60	3	3	117.64	11.50
8	1700	60	9	3	124.31	9.66
9	1500	60	6	1	122.34	11.42
10	1900	60	6	1	119.06	9.96
11	1500	60	6	3	120.21	11.02
12	1900	60	6	3	115.37	9.11
13	1700	30	3	2	107.34	11.90
14	1700	90	3	2	106.13	12.22
15	1700	30	9	2	116.31	9.76
16	1700	90	9	2	112.31	10.42
17	1500	60	3	2	118.52	12.48
18	1900	60	3	2	115.98	9.72
19	1500	60	9	2	122.66	9.92
20	1900	60	9	2	124.22	9.20
21	1700	30	6	1	115.32	10.42
22	1700	90	6	1	104.34	12.12
23	1700	30	6	3	110.27	9.62
24	1700	90	6	3	108.31	10.56
25	1700	60	6	2	138.40	12.24
26	1700	60	6	2	143.64	12.30
27	1700	60	6	2	139.21	12.46
28	1700	60	6	2	139.28	12.98
29	1700	60	6	2	139.91	12.70
30	1700	60	6	2	141.34	13.70

presented in Table 3. The fractured test pieces were subjected to scanning electron microscopic examination to identify the mode of fracture. The observed SEM Images are presented in Fig. 4. A ductile mode of

fracture was identified on the fractured zone if the test pieces were fabricated using the rotating tool equipped with a square pin. Some defective test pieces are magnified to identify the type of defect on the weld



Fig. 3: Tensile tested specimen

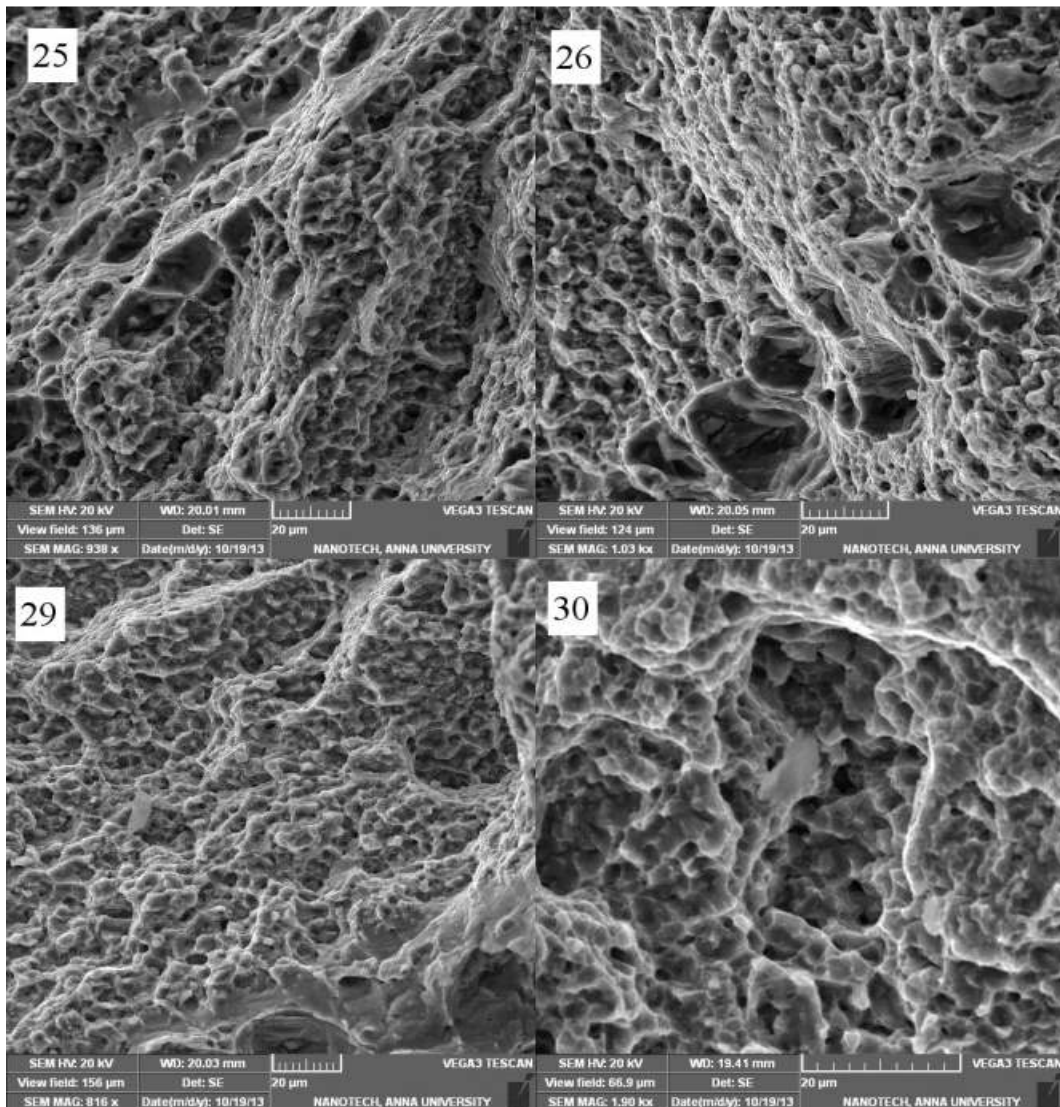


Fig. 4: Fracture SEM zone of 25, 26, 29 and 30th run samples

macro defects consequences a drastic reduction in tensile strength of 44% on AA 2024 and 51% joints. Figure 5 reveals the macro defects in fractured samples from the fabricated weld joints. These







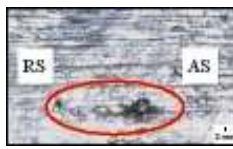


Input parameters	Parameter range	Macrostructure	Name of the defect	Probable reason
Rotational speed	1500 rpm		Tunnel defect	Insufficient heat generation and metal transportation
	1700 rpm		Pin holes	Due to low frictional generational
	1900 rpm		Tunnel defect	Insufficient heat generation and metal transportation
Welding speed	30 mm/min		Pin holes	Due to low frictional generational
	60 mm/min		Pin holes	Due to low frictional generational
	90 mm/min		Tunnel defect	Insufficient heat generation and metal transportation
Axial load	3 kN		Kissing bond	Insufficient stirring butt surfaces
	6 kN		Pin holes	Due to low frictional generational
	9 kN		Worm hole	High frictional heat generation

Fig. 5: Macrostructure observation of FS welded specimens

on AA 6061 aluminum alloys against the base material strength.

METHODOLOGY

Response Surface Methodology (RSM): Researchers always look the feasible solution for the optimum boundary region. The optimum values may be either maximum or minimum of a particular function that depends upon the input process parameters. The graphical presentation of proposed methodology which is employed based on response surface methodology using desirability approach is presented in Fig. 6. Response Surface Methodology (RSM) is a combination mathematical and statistical technique for analyzing the complex problems in which several independent variables influence a dependant variable or the goal is to optimize the response (Montgomery, 1980). In many situations in industries, the independent factors can be written as in quantitative form as in Eq. (1). Then these independent factors can be thought of having a functional relationship as follows:

$$Y = \varphi(a_1, a_2, a_3, \dots, a_n) \pm \text{Experiemtnal Error}$$

Between the response Y and quantitative factors of $a_1, a_2, a_3 \dots a_n$, the function ‘ Φ ’ is called response surface or response function. A response surface can be responded to the given set of independent factors. When the ‘ Φ ’ is unknown, it can be approximated satisfactorily by polynomial within the experimental region. In the present investigation, RSM is applied to formulate the mathematical model in the form of the multiple regression equation for the quality characteristics of tool pin profile on friction stir welded AA2024-AA6061 aluminum alloys. In this method, the independent variables are viewed as a surface to which a mathematical model is fitted.

The Ultimate Tensile Strength (UTS) and Tensile Elongation (TE) of dissimilar weld joints composed of AA6061-AA2024 aluminum alloys are related to the rotational speed (N), the welding speed (F), axial load (P) and Pin Shape (PS). The surface is represented by the following:

$$UTS = f(N, F, P, PS) \tag{1}$$

$$TE = f(N, F, P, PS) \tag{2}$$

A second-order polynomial regression equation is used to represent the response surface ‘Y’ for K factors:

$$Y = \beta_o + \sum_{i=1}^k \beta_i x_i + \sum_{i=1}^k \beta_{ii}^2 x_i^2 + \sum_{i < j} \beta_{ij} x_i x_j + \epsilon \tag{3}$$

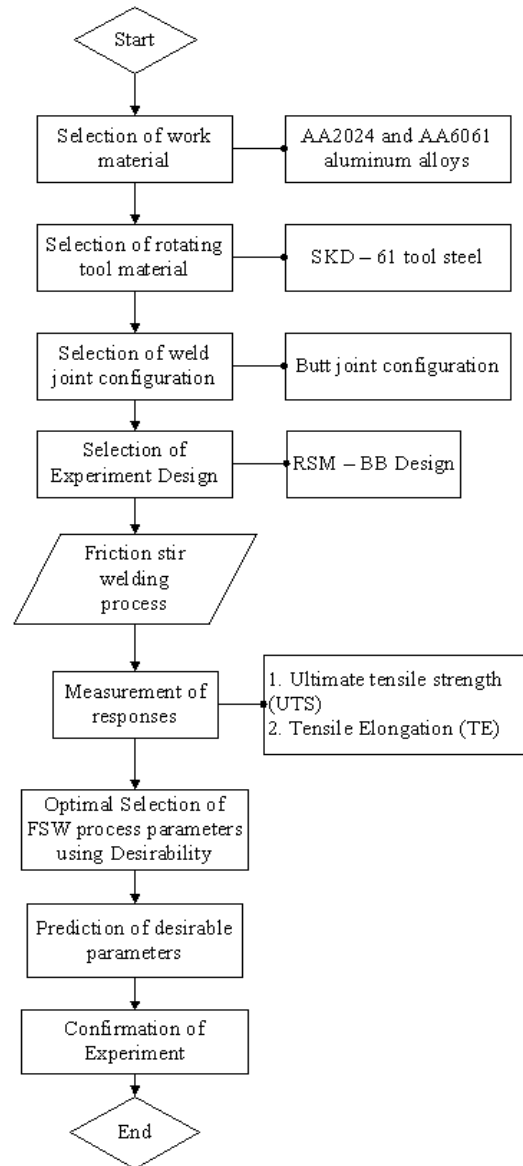


Fig. 6: Graphical demonstration of present RSM coupled with desirability approach

where, β_o is the average response, $\beta_i, \beta_{ii}, \beta_{ij}$ is the coefficients that depend on the major and interaction effects of the parameters and ϵ is the statistical error. A second-order model is useful when approximating the true response surface in a relatively small region near the center point of response surface. This area exhibits a substantial curvature in the true response function ‘ f ’; this function is very flexible, allowing it to take various functional forms by approximating the true response surface. Estimating the β values in the second-order model using the least squares method is easy; in addition, numerous reports indicate that the second-order model will work well for real-time engineering problems (Design Expert, 2005). The values of the polynomial coefficients are calculated using the Design

Expert version 8 statistical software. Therefore, the regression coefficients of the second-order polynomial equation are obtained. The coded equations are presented in Eq. (4) and (5):

$$\text{Ultimate Tensile Strength (UTS)} = - 902.25563 + 1.03486 \text{ Rotational speed} + 200.07119 \text{ Welding speed} + 12.33048 \text{ Axial load} + 32.16226 \text{ Pin Shape}$$

$$- 0.023200 \text{ Rotational speed} \times \text{Welding speed} + 4.51000 \text{ Welding speed} \times \text{Pin Shape} - 2.99551E - 004 \text{ Rotational speed}^2 - 86.94310 \text{ Welding speed}^2 - 0.93717 \text{ Axial load}^2 - 9.46577 \text{ Pin Shape}^2 \quad (4)$$

$$\text{Tensile Elongation (TE)} = - 73.10948 + 0.096367 \text{ Rotational speed} + 7.03905 \text{ Welding speed} - 0.31669 \text{ Axial load} + 5.21411 \text{ Pin Shape} +$$

Table 4: Experimental vs. predicted values of Ultimate Tensile Strength (UTS), Tensile Elongation (TE)

Exp No.	Ultimate tensile strength (Mpa)			Tensile elongation (%)		
	Experimental value	Predicted value	Error (%)	Experimental value	Predicted value	Error (%)
1	108.31	108.17	0.13	10.64	10.61	0.30
2	109.33	110.08	-0.69	9.12	9.13	-0.07
3	109.32	108.57	0.68	11.64	11.71	-0.61
4	101.06	101.21	-0.15	9.62	9.73	-1.14
5	122.25	121.22	0.84	12.64	12.57	0.54
6	127.09	126.81	0.22	9.64	10.01	-3.89
7	117.64	117.92	-0.24	11.50	11.20	2.58
8	124.31	125.35	-0.83	9.66	9.81	-1.51
9	122.34	121.44	0.74	11.42	11.40	0.22
10	119.06	119.50	-0.37	9.96	9.89	0.72
11	120.21	119.84	0.31	11.02	10.83	1.71
12	115.37	116.34	-0.84	9.11	8.88	2.58
13	107.34	108.72	-1.29	11.90	11.59	2.59
14	106.13	105.88	0.23	12.22	12.28	-0.45
15	116.31	116.62	-0.27	9.76	9.45	3.23
16	112.31	110.99	1.17	10.42	10.47	-0.46
17	118.52	119.44	-0.78	12.48	12.79	-2.45
18	115.98	114.67	1.13	9.72	10.03	-3.23
19	122.66	123.90	-1.01	9.92	9.79	1.32
20	124.22	123.23	0.80	9.20	9.08	1.34
21	115.32	115.09	0.20	10.42	10.55	-1.24
22	104.34	106.34	-1.92	12.12	11.78	2.79
23	110.27	108.20	1.88	9.62	10.14	-5.41
24	108.31	108.47	-0.15	10.56	10.61	-0.51
25	138.40	140.73	-1.68	12.24	12.75	-4.18
26	143.64	140.73	2.03	12.30	12.75	-3.67
27	139.21	140.73	-1.09	12.46	12.75	-2.34
28	139.28	140.73	-1.04	12.98	12.75	1.76
29	139.91	140.73	-0.58	12.70	12.75	-0.40
30	141.34	140.73	0.43	13.70	12.75	6.92

Table 5: ANOVA results for Ultimate Tensile Strength (UTS), Tensile Elongation (TE) and statistical results of the developed model

Source	S.S.	DOF	M.S.	F-value	p-value	
ANOVA for Ultimate Tensile Strength (UTS)						
Model	4764.60	14	340.33	111.64	<0.0001	Significant
A-rotational speed*	22.25	1	22.25	7.30	0.0157	
B-welding speed*	53.81	1	53.81	17.65	0.0007	
C-axial load*	127.01	1	127.01	41.66	<0.0001	
D-pin shape*	17.02	1	17.02	5.58	0.0311	
AB*	21.53	1	21.53	7.06	0.0172	
AC	4.20	1	4.20	1.38	0.2575	
AD	0.61	1	0.61	0.20	0.6611	
BC	1.95	1	1.95	0.64	0.4360	
BD*	20.34	1	20.34	6.67	0.0200	
CD	0.84	1	0.84	0.27	0.6074	
A ² *	1026.36	1	1026.36	336.67	<0.0001	
B ² *	3377.47	1	3377.47	1107.89	<0.0001	
C ² *	508.58	1	508.58	166.83	<0.0001	
D ² *	640.55	1	640.55	210.12	<0.0001	
Residual	48.78	16	3.05			
Lack of fit	22.82	10	2.28	0.53	0.8228	Not significant
Pure error	25.96	6	4.33			
Cor total	4813.38	30				

Table 5: (Continue)

ANOVA for Tensile Elongation (TE)						
Model	53.55	14	3.83	22.51	<0.0001	Significant
A-rotational speed*	9.00	1	9.00	52.94	<0.0001	
B-welding speed*	2.18	1	2.18	12.86	0.0025	
C-axial load*	11.72	1	11.72	68.98	<0.0001	
D-pin shape*	1.86	1	1.86	10.97	0.0044	
AB	0.06	1	0.06	0.37	0.5527	
AC*	1.04	1	1.04	6.12	0.0249	
AD	0.05	1	0.05	0.30	0.5927	
BC	0.03	1	0.03	0.17	0.6855	
BD	0.14	1	0.14	0.85	0.3703	
CD	0.34	1	0.34	1.98	0.1786	
A ² *	15.89	1	15.89	93.49	<0.0001	
B ² *	6.68	1	6.68	39.33	<0.0001	
C ² *	5.04	1	5.04	29.65	<0.0001	
D ² *	7.34	1	7.34	43.19	<0.0001	
Residual	2.72	16	0.17			
Lack of fit	1.20	10	0.12	0.47	0.8592	Not significant
Pure error	1.52	6	0.25			
Cor total	56.27	30				

Statistical results of the developed model

Response	R ²	Adj. R ²	Predicted R ²
Ultimate Tensile Strength (UTS)	0.9899	0.9810	0.9654
Tensile Elongation (TE)	0.9517	0.9094	0.8406

*: Significant factor; S.S.: Sum of square; M.S.: Mean square

$$\begin{aligned}
 &5.29167E - 004 \text{ Rotational speed} \times \text{Axial load} - \\
 &1.58750E - 003 \text{ Rotational speed} \times \text{Pin Shape} - \\
 &2.95074E - 005 \text{ Rotational speed}^2 - 3.24119 \\
 &\text{Welding speed}^2 - 0.070450 \text{ Axial load}^2 - 0.72405 \\
 &\text{Pin Shape}^2 \quad (5)
 \end{aligned}$$

The predicted values for the ultimate tensile strength, tensile elongation and their deviations are presented in Table 4. The developed model is verified using the results of an Analysis of Variance (ANOVA) at a 95% confidence level. The results of the ANOVA are presented in Table 5. The higher level of the ‘R-Sq’ and lower Predicted R-Squared’ and Adj. R-Squared’ values reveal the adequacy of the model. Therefore, the obtained ‘R-Sq’ and ‘Predicted R-Squared’ values agree with the ‘Adj. R-Squared’ values, thereby confirming the adequacy of the present model. The results of the ANOVA indicate that the selected process parameters are significant factors that affect the ultimate tensile strength and tensile elongation. Using a scatter diagram, the adequacy of the model is validated further. The scatter diagram of the normal plot of the predicted versus actual values for the ultimate tensile strength and tensile elongation is shown in Fig. 7a and b. The similar values of the predicted and actual values are fitted on a 45° scatter line, thus further validating the present model. In addition, the predicted values are within ±10% error; therefore, the obtained model fits the experiment.

Desirability approach: The optimum points did not coincide in all cases when the process has multi responses. In such conditions, several statistical methods used for solving multi response problems such as overlaying the contour plot for each response, constrained optimization problems and the desirability

approach (Zhang *et al.*, 2005). The multi response optimization process is balancing the responses when the number of responses is two or more than two. The main objective of this research is to maintain the balance between the productivity and product quality. In this study, the productivity factors are rotational speed, welding speed, axial load and pin shapes. Similarly, the quality factors are the ultimate tensile strength and tensile elongation of the fabricated joints. An appropriate selection of productivity factors will achieve the high production rate. Therefore, the productivity factors are playing a vital role in the mass production industries. Quality factors deals in this study are ultimate tensile strength and tensile elongation. Since these factors are very much useful for the precision industries such as aerospace, ship building etc. But these factors are opposite in nature. If rotational speed and axial load is increased, then ultimate tensile strength is increased rather tensile elongation of the welded joint is reduced. Therefore, for these kinds of diversified responses, Derringer and Suich (1980) demonstrated a technique called desirability. It is very useful technique for the research and mass production industries where the productivity and quality factors have high conflict between one another:

$$D(X) = (d_1 \times d_2 \times d_3 \dots d_n)^{\frac{1}{m}} = (\prod_{i=1}^n d_n)^{\frac{1}{m}}$$

This approach uses an objective function, D (X), called desirability function and converted into a scale free value (d_n) called individual desirability; m is the number of responses. The desirable ranges are from 0 to 1.0 indicated one or more responses are outside their acceptable limits and 1 indicates the response is in the ideal case.

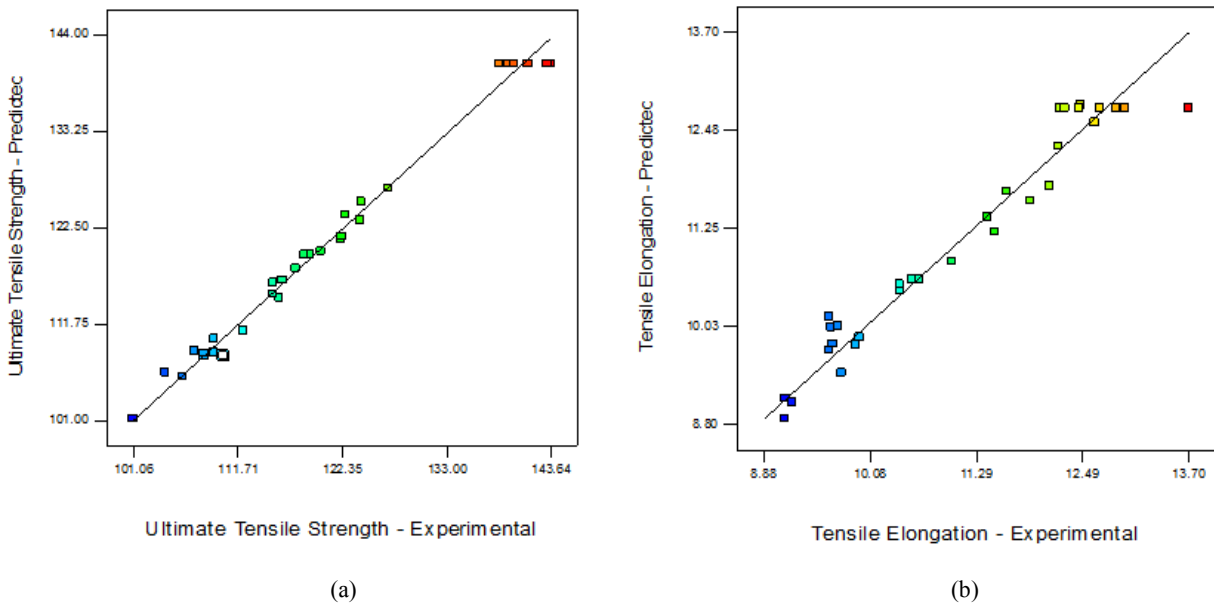


Fig. 7: Experimental vs. predicted plot for ultimate tensile strength, tensile elongation

RESULTS AND DISCUSSION

Using the regression models, the effects of each parameter on the ultimate tensile strength and tensile elongation are visualized using the response surface plot from 5a and b to 7a and b.

Identifying a suitable rotating pin profile for generating a sound weld via a frictional heat and hydrostatic pressure is important; specifically, this pin profile must thoroughly blend dissimilar materials along the weld line. In the surface plots, the ultimate tensile strength of the fabricated weld joints is lower than that of the base metals, regardless of the process parameters. In addition, when the process parameters induce low frictional heat and high material flow, the fabricated welded joints exhibit a lower tensile strength.

The tensile elongation decreases when increasing the rotational speed and axial load; this value increases when increasing the welding speed. The strengthening precipitates cluster toward the Thermo-Mechanically Affected Zone (TMAZ), Heat-Affected Zone (HAZ) and Weld Nugget (WN), demonstrating material flow on the TMAZ and WN; therefore, lower tensile strength is observed on the fabricated joints that are composed of dissimilar aluminum alloys (AA6061-AA2024) (Kalaiselvan and Murugan, 2013). Figure 8a and b show the perturbation plot of the ultimate tensile strength and tensile elongation. This perturbation plot compares the effect of every factor at a particular point in the design space (Design Expert, 2005). The possible situations that affect the tensile strength and elongation are discussed below.

Effect of pin shapes: For the dissimilar aluminum alloys (AA2024-AA6061), utilizing a square pin profile imparts higher tensile strength and tensile elongation

than to the tapered and cylindrical pin profiles. The rotating tool pin with flat faces produces large pulsating effects, increasing the ultimate tensile strength (Elangovan *et al.*, 2008). Therefore, the rotating tools equipped with square pins impart high ultimate tensile strength, while the cylindrical and taper pins impart low tensile strength. A similar behavior was observed in all of the experiments. Figure 9a and b to 11a and b show graphical representations of the effects of the process parameters for each pin profile using surface plots. The surface plots are three-dimensional representations of the response to the selected factors (Design Expert, 2005). Therefore, each pin shape and process parameter were plotted to demonstrate its behavior regarding the ultimate tensile strength and tensile elongation.

Effects of tool rotational speed: Increasing the rotational speed of the tool increases the tensile strength of the joints. Figure 9a shows a response surface graph that reveals the effects of the rotational speed of the tool for each pin profile. The surface plot forms a mound shape or a simple maximum surface (Robert *et al.*, 2003). For the simple maximum type, the response values increase gradually from the stationary edge. Similarly, the tensile strength is increased when the rotational speed gradually increases to the stationary edge (center of surface plot). The lower rotational speed (1500 rpm) generates poor material flow, thereby imparting low tensile strength and coarsening the strengthening precipitates. Re-precipitation, a lowered dislocation density and solubilization at the weld zone decreases the tensile strength of fabricated joints when at the maximal rotational speed (1900 rpm), thus producing surface defects and micro voids (Robert *et al.*, 2003; Li *et al.*, 2012; Hui-Jie *et al.*, 2013). These

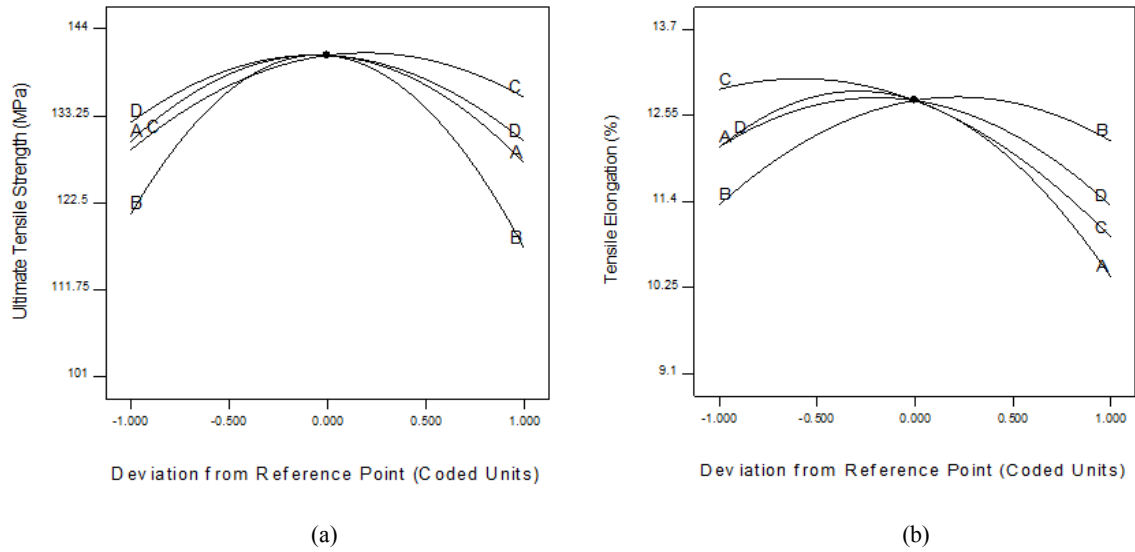


Fig. 8: Perturbation plot for ultimate tensile strength, tensile elongation

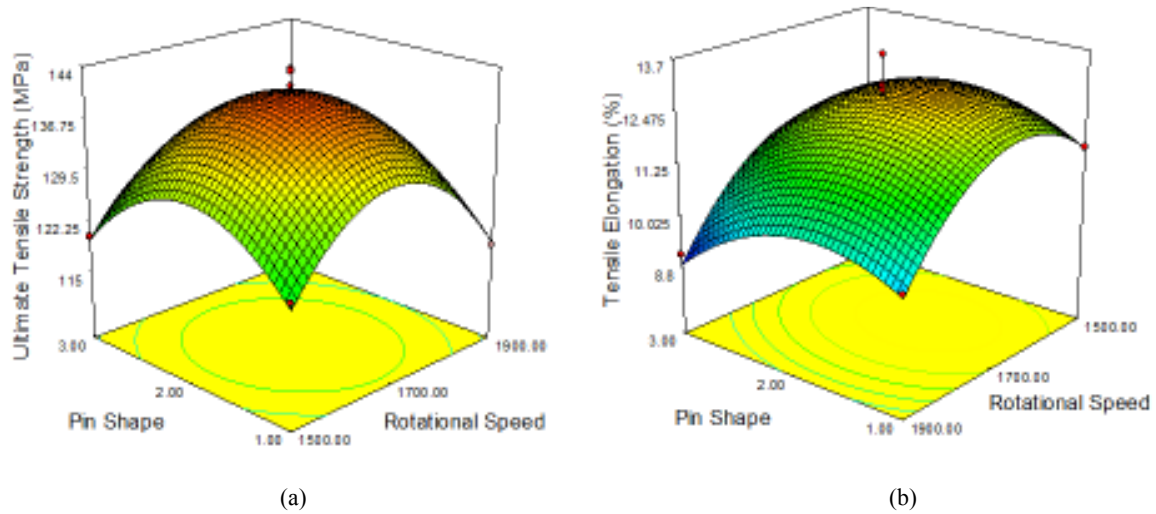


Fig. 9: Surface plot of rotational speed, pin shape vs. ultimate tensile strength, tensile elongation

effects were observed in all of the experiments, even when the rotating tool was equipped with flat faces (square pin). The weld joints have low tensile strength if they are fabricated using tapered and cylindrical rotating pins. Therefore, the joints fabricated by square pins have more ultimate tensile strength than the other pin profiles.

Figure 9b shows a three-dimensional representation of the rotational speed (N) and pin shapes vs. tensile elongation. A rising ridge (Design Expert, 2005) surface plot is generated from the experimental results. The tensile elongation decreases when increasing the rotational speed. Therefore, the rotational speed encourages the clustering among the strengthening precipitates due to the plastic flow in the weld nugget, the thermo mechanical affected zone and the heat affected zone, regardless of the pin shape (Flores *et al.*,

1998; Murr *et al.*, 1998; Su *et al.*, 2003; Sato *et al.*, 2003; Srivatsan *et al.*, 2007; Sanjay *et al.*, 2012). Therefore, an increase in the rotational speed decreases the tensile elongation of the dissimilar aluminum alloys (AA 6061 and AA 2024) in welded joints. The tool equipped with the square pin exhibits the highest tensile elongation; the second-highest tensile elongation was observed with the tapered pin.

Effects of the welding speed: The effects of the welding speed for dissimilar aluminum alloys (AA 6061-AA 2024) joined by friction stir welding are shown in response Fig. 9a, which shows the effects of the welding speed vs. the pin shape. The obtained surface plot is a ‘mound shape or simple maximum’ (Design Expert, 2005). The tensile strength is increased when the welding speed increases to 60 mm/min. Then,

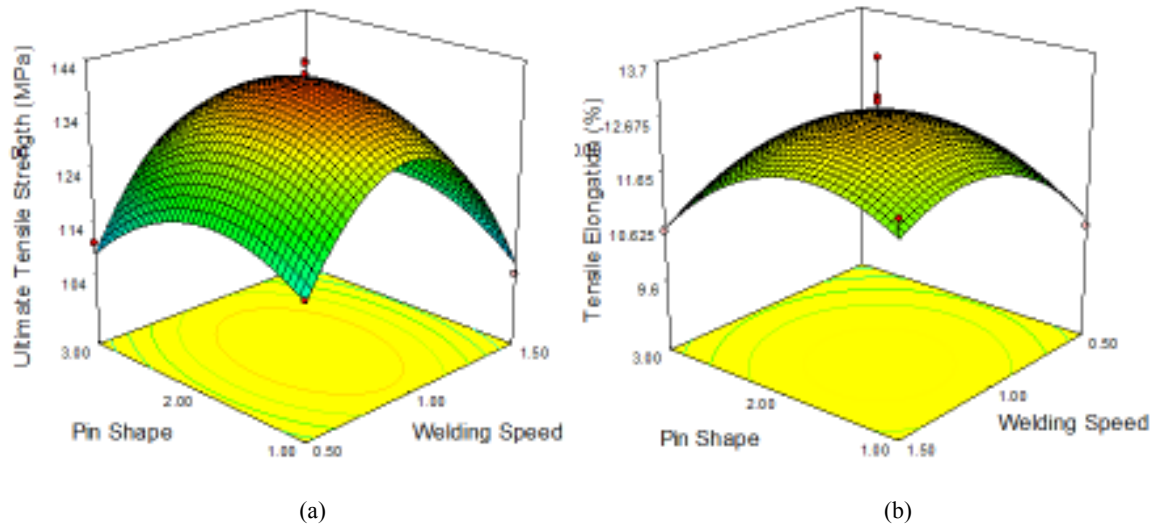


Fig. 10: Surface plot of welding speed, pin shape vs. ultimate tensile strength, tensile elongation

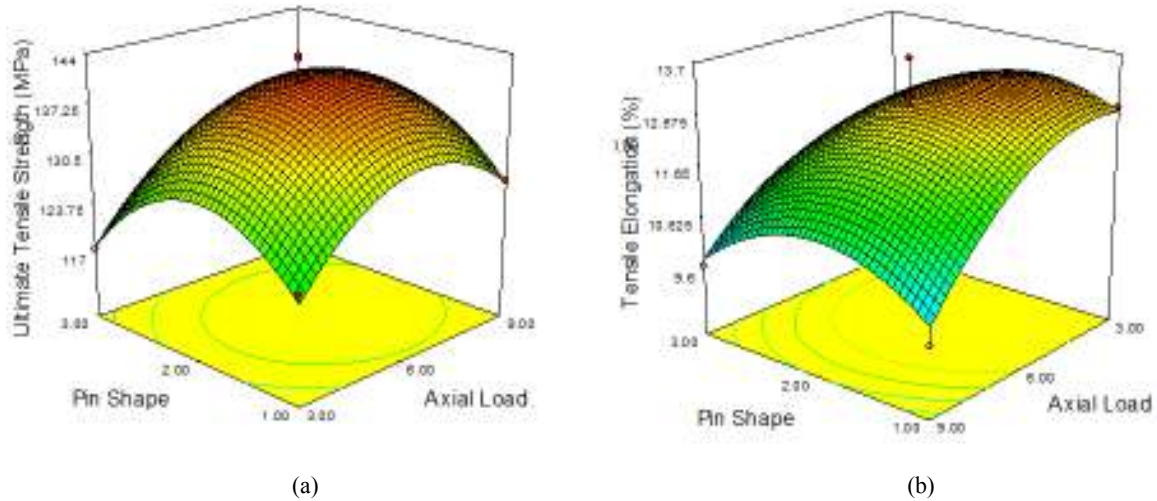


Fig. 11: Surface plot of axial load, pin shape vs. ultimate tensile strength, tensile elongation

the tensile strength decreases when gradually increasing the welding speed to 90 mm/min, regardless of the tool pin shape, due to the increased frictional heat and insufficient heat generation at lower and higher welding speeds (Kumar and Kailas, 2008). The welding speed at the lowest levels (30 mm/min) causes metallurgical transformations that result in poor joint strength. This behavior contributes to the tunneling defects, even at a higher welding speed and pin holes at lower welding speeds (Sato *et al.*, 2003).

The response graphs for the rotational speed (N) and pin shape vs. tensile elongation are shown in Fig. 10b. The obtained surface plot is a ‘rising ridge’ type (Design Expert, 2005). Increasing the welding speed increases the tensile elongation. The welding speed discourages clustering among the strengthening precipitates, regardless of the tool pin shape (Flores *et al.*, 1998; Murr *et al.*, 1998; Su *et al.*, 2003; Sato

et al., 2003; Srivatsan *et al.*, 2007; Sanjay *et al.*, 2012). The pin shapes (e.g., taper, square, cylinder) enhance the material flow, thereby generating localized strain. Therefore, an increase in the welding speed increases the tensile elongation of the friction stir welded AA 6061 and AA 2024 aluminum alloys, regardless of the tool pin shape.

Effects of axial load: A three-dimensional response surface plot 10 (a) represents the effect of the axial load and pin shapes vs. ultimate tensile strength. The obtained shape of the surface plot is a ‘simple maximum’ (Design Expert, 2005). The increased axial load increases the joint strength of the specimen to an axial force of 6 kN. Beyond that point, the joint strength gradually decreases when increasing the axial load (Flores *et al.*, 1998; Zhang *et al.*, 2005; Kumar and Kailas, 2008). The higher axial force allowed the tool to

plunge into the work piece easily, thereby increasing the plunge depth and generating additional frictional heat. In addition, the higher plunge depth encourages clustering among the strengthening particles and the material flow, imparting adequate joint strength on the fabricated weld joints, regardless of the tool pin profile. Moreover, the lower axial force generates insufficient heat levels because the axial load is directly responsible for the frictional heat generation; this situation results in

poor material flow, while a higher axial load produces an excessive material flow along the weld line, increasing the size of the weld nugget (Zhang *et al.*, 2005; Kumar and Kailas, 2008). Similar behavior was observed with the tools equipped with tapered and cylinder pin profiles.

Figure 11b presents the three-dimensional surface plot describing the effects of axial load and pin shapes vs. tensile elongation. The obtained surface plot is a

Table 6: Predicted vs. observed optimum values of responses through desirability

Response	Goal	Range		Importance
		Lower limit	Upper limit	
Rotational speed (N) (rpm)	-	1500	1900	5
Welding speed (F) (mm/min)	-	30	90	5
Axial load (P) (kN)	-	3	9	5
Pin Shape (PS)	-	St. Cyl (SC)	Squ (SQ) Tap (TA)	5
Ultimate Tensile Strength (UTS) (MPa)	Maximize	101.06	143.64	5
Tensile Elongation (TE) (%)	Maximize	9.11	12.53	5

Table 7: Desirable values

Rotational speed (N) (rpm)	Welding speed (F) (mm/min)	Axial load (P) (kN)	Pin Shape (PS)	Ultimate tensile strength (MPa)	Tensile elongation (%)	Desirability	
1666.91	59.90	5.72	1.88	140.266	12.53	0.960	Selected
1667.22	59.85	5.73	1.87	140.264	12.53	0.960	
1667.40	59.93	5.71	1.89	140.264	12.53	0.960	
1666.82	59.82	5.73	1.88	140.264	12.53	0.960	
1665.19	60.11	5.74	1.88	142.264	12.53	0.960	
1666.90	60.25	5.70	1.88	140.262	12.53	0.960	
1665.83	59.56	5.73	1.90	140.261	12.53	0.959	
1665.88	60.26	5.72	1.88	140.260	12.53	0.959	
1667.56	60.09	5.70	1.89	140.259	12.53	0.959	
1669.56	59.81	5.71	1.88	140.259	12.53	0.959	

Table 8: Predicted vs. observed optimum values of responses through desirability

Response	Goal	Predicted	Observed	Error (%)
Ultimate Tensile Strength (UTS) (MPa)	Maximize	140.266	138.17	1.49
Tensile Elongation (TE) (%)	Maximize	12.530	11.81	5.74

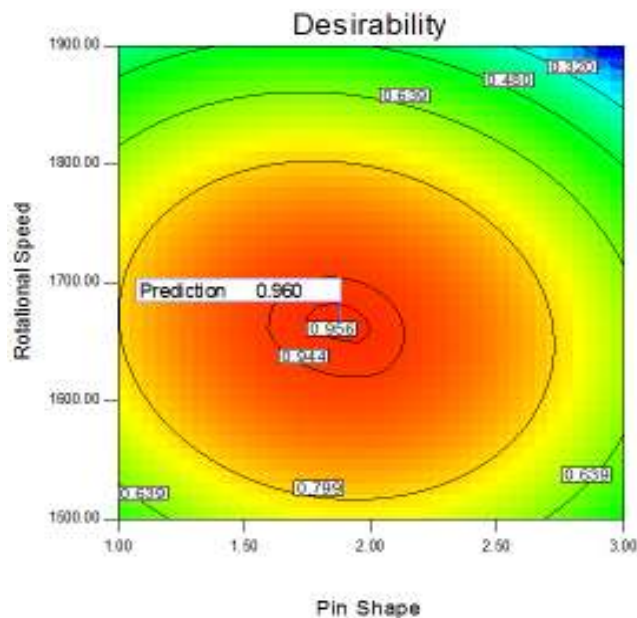


Fig. 12: Contour plot of overall desirability function

'rising ridge' type. The axial load is vital for the frictional heat generation and the plunging depth of the tool pin profile (Flores *et al.*, 1998; Zhang *et al.*, 2005; Kumar and Kailas, 2008). Therefore, increasing the axial load encourages clustering among the strengthening precipitates, thus reducing the tensile elongation on the weld joints between AA 6061 and AA 2024 aluminum alloys, regardless of the pin shapes.

Multi response optimization of process parameters through desirability: Composite desirability is the weighted geometric mean of the individual desirability for the responses. The factor settings with maximum total desirability are considered to be the optimal parameter conditions. The simultaneous objective function is a geometric mean of all transformed responses (Derringer and Suich, 1980; Zhang *et al.*, 2005). This combination has been evaluated with the help of the Design Expert Software. Two responses such as ultimate tensile strength, tensile elongation have been used to optimize simultaneously using developed mathematical model Eq. (4) and (5) based on desirability function. In a multi response domain, a measure of how the solution has satisfied the combined goals for all responses must be assured. The optimality solution is to evaluate the input process parameters in experiment range for maximizing ultimate tensile strength and tensile elongation of the fabricated welded joints. The input parameter their ranges, goals and predicted desirable values of responses under prescribed conditions presented in Table 6 and 7 and its graphical representation of contour plot is presented in Fig. 12.

Once the optimal process input parameters are selected then the final step is to predict and verify the improvement of the performance characteristic using the optimal level of the friction stir welding parameters. Then the confirmation of experiments was conducted in order to verify the predicted friction stir welding parameters of the optimal parametric setting for ultimate tensile strength and tensile elongation. Table 8 show the percentage of error of the developed models for the responses with optimal parameter setting during FS welding process. In Table 8, it can be observed that the calculated error is small. Obviously, this confirms excellent reproducibility of the experimental conclusions.

CONCLUSION

Based on the present study, the following theoretical and experimental conclusions can be drawn:

- The mathematical models were developed at 95% confidence level for the desired parameters such as rotational speed (N), welding speed (F), axial load (P) by varying the pin shapes.

- The ultimate tensile strength of the fabricated welded joints is lower than the base materials (AA 6061 and AA 2024 aluminum alloys).
- The increased rotational speed (N) and axial load (P) parameters decrease the tensile elongation, while the tensile elongation increases after increasing the welding speed (F), regardless of the pin shape.
- The increased axial load increases the friction heat generation and the plunging of the tool pin, promoting clustering among the strengthening precipitates. Therefore, higher tensile strengths were obtained using the fabricated weld joints.
- The conformability of the predicted results indicate that the mathematical model and the application of the RSM technique are sufficient when studying the friction stir welding process with AA 6061 and AA 2024 aluminum alloys.
- The rotating tools equipped with square pins are vital in this study during frictional heat generation; this pin profile is influential during the development of tensile strength in weld joints fabricated from AA 6061 and AA 2024 aluminum alloys.

Therefore, the present investigation findings along with various mathematical models will provide effective guideline to select parameter settings for achieving desired ultimate tensile strength and tensile elongation during friction stir welding of aluminum alloys of AA 2024 and AA 6061.

ACKNOWLEDGMENT

The authors are grateful to Sri Chandrasekharendra Saraswathi Viswa Maha Vidyalaya, Enathur, Kanchipuram, Tamilnadu for funding this research work under a university minor research project. The authors also thank Mr. K. Rangan, Metal Joining Lab, I.I.T Madras for his technical assistance.

REFERENCES

- Anish, K., K. Vinod and K. Jatinder, 2013. Multi-response optimization of process parameters based on response surface methodology for pure titanium using WEDM process. *Int. J. Adv. Manuf. Tech.*, 68(9-12): 2645-2668.
- ASM Handbook, 1990. Properties and Selection: Non Ferrous Alloys and Special Purpose Materials. ASM International, Vol. 2.
- Biswas, P., D.A Kumar and N.R. Mandal, 2012. Friction stir welding of aluminum alloy with varying tool geometry and process parameters. *J. Eng. Manufacture*, 226(4): 641-649.

- Da Silva, A.A.M., E. Arruti, G. Janeiro, E. Aldanondo, P. Alvarez and A. Echeverria, 2011. Material flow and mechanical behaviour of dissimilar AA2024-T3 and AA7075-T6 aluminium alloys friction stir welds. *Mater. Des.*, 32(4): 2021-2027.
- Dawes, C. and W. Thomas, 1995. Friction stir joining of aluminium alloys. *TWI Bull.*, 6: 124-127.
- Dehghani, M., S.A.A. Akbari Mousavi and A. Amadeh, 2013. Effects of welding parameters and tool geometry on properties of 3003-H18 aluminum alloy to mild steel friction stir weld. *T. Nonferr. Metal. Soc.*, 23(7): 1957-1965.
- Derringer, G. and R. Suich, 1980. Simultaneous optimization of several response variables. *J. Qual. Technol.*, 12(4): 214-219.
- Design Expert, 2005. User Manual Reference-Stat-Ease, Inc., 2005.
- Elangovan, K., V. Balasubramanian and M. Valliappan, 2008. Influences of pin profile and axial force on the formation of friction stir processing zone in AA6061 aluminium alloy. *Int. J. Adv. Manuf. Tech.*, 38(3-4): 285-294.
- Elmesalamy, A.S., L. Li, J.A. Francis and H.K. Sezer, 2013. Understanding the process parameter interactions in multiple-pass ultra-narrow-gap laser welding of thick-section stainless steels. *Int. J. Adv. Manuf. Tech.*, 68: 1-17.
- Flores, O.V., C. Kennedy, L.E. Murr, D. Brown, S. Pappu and B.M. Nowak, 1998. Microstructural issues in a friction-stir-welded aluminum alloy. *Scripta Materialia.*, 38(5): 703-708.
- Hu, Z.L., X.S. Wang and S.J. Yuan, 2012. Quantitative investigation of the tensile plastic deformation characteristic and microstructure for friction stir welded 2024 aluminum alloy. *Mater. Charact.*, 73: 114-123.
- Hui-jie, Z., L. Hui-jie and Y. Lei, 2013. Thermal modeling of underwater friction stir welding of high strength aluminum alloy. *T. Nonferr. Metal. Soc.*, 23(4): 1114-1122.
- Jayaraman, M. and V. Balasubramanian, 2013. Effect of process parameters on tensile strength of friction stir welded cast A356 aluminium alloy joints. *T. Nonferr. Metal. Soc.*, 23(3): 605-615.
- Kalaiselvan, K. and N. Murugan, 2013. Role of friction stir welding parameters on tensile strength of AA6061-B₄C composite joints. *T. Nonferr. Metal. Soc.*, 23(3): 616-624.
- Karthikeyan, R. and V. Balasubramanian, 2010. Predictions of the optimized friction stir spot welding process parameters for joining AA2024 aluminum alloy using RSM. *Int. J. Adv. Manuf. Tech.*, 51: 173-183.
- Kumar, K. and S.V. Kailas, 2008. On the role of axial load and the effect of interface position on the tensile strength of a friction stir welded aluminium alloy. *Mater. Design.*, 29(4): 791-797.
- Kwon, J.W., M.S. Kang, S.O. Yoon, Y.J. Kwon, S.T. Hong, D.I. Kim, K.H. Lee, J.D. Seo, J.S. Moon and K.S. Han, 2012. Influence of tool plunge depth and welding distance on friction stir lap welding of AA5454-O aluminum alloy plates with different thicknesses. *T. Nonferr. Metal. Soc.*, 22(3): 624-628.
- Lakshminarayanan, A.K. and V. Balasubramanian., 2008. Process parameters optimization for friction stir welding of RDE-40 aluminium alloy using Taguchi technique. *T. Nonferr. Metal. Soc.*, 18(3): 548-554.
- Lee, W.B., Y.M. Yeon and S.B. Jung, 2003. The improvement of mechanical properties of friction-stir-welded A356 Al alloy. *Mater. Sci. Eng. A*, 355(1-2): 154-159.
- Li, R.D., J.L. Li, J.T. Xiong, F.S. Zhang, K. Zhao and C.Z. Ji, 2012. Friction heat production and atom diffusion behaviors during Mg-Ti rotating friction welding process. *T. Nonferr. Metal. Soc.*, 22(11): 2665-2671.
- Lomolino, S., R. Tovo and J. Dos Santos, 2005. On the fatigue behavior and design curves of friction stir butt welded Al alloys. *Int. J. Fatigue*, 27: 305-316.
- Mohammadtaheri, M., M. Haddad-Sabzevar, M. Mazinani and E. Bahrami Motlagh., 2013. The effect of base metal conditions on the final microstructure and hardness of 2024 aluminum alloy friction-stir welds. *Metall. Mater. Trans. B*, 44(3):738-743.
- Montgomery, D.C., 1980. *Design and Analysis of Experiments*. 4th Edn., Wiley, New York.
- Muhammad, N., Y.H.P. Manurung, R. Jaafar, S.K. Abas, G. Tham and E. Haruman, 2013. Model development for quality features of resistance spot welding using multi-objective Taguchi method and response surface methodology. *J. Intell. Manuf.*, 24: 1175-1183.
- Murr, L.E., G. Liu and J.C. Mc Clure, 1998. A TEM study of precipitation and related microstructures in friction-stir-welded 6061 aluminum. *J. Mater. Sci.*, 33(5): 1243-1251.
- Ouyang, J.H. and R. Kovacevic, 2002. Material flow and microstructure of the friction stir butt welds of the same and dissimilar aluminum alloys. *J. Mater. Eng. Perform.*, 11(1): 51-63.
- Rajakumar, S. and V. Balasubramanian, 2012. Multi-response optimization of friction-stir-welded AA1100 aluminum alloy joints. *J. Mater. Eng. Perform.*, 21: 809-822.
- Rhodes, C.G., M.W. Mahoney and W.H. Bingel, 1997. Effect of friction stir welding on microstructure of 7075 aluminium. *Scripta Mater.*, 36: 69-75.
- Robert, L.M., F.G. Richard and L.H. James, 2003. *Statistical Design and Analysis of Experiments: With Applications to Engineering and Science*. 2nd Edn., J. Wiley, Hoboken, N.J.

- Sanjay, K., K. Sudhir and K. Ajay, 2012. Optimization of process parameters for friction stir welding of joining A6061 and A6082 alloys by Taguchi method. *J. Mech. Eng. Sci.*, 227(6): 1150-1163.
- Sato, Y.S., M. Urata, H. Kokawa and K. Ikeda, 2003. Hall-petch relationship in friction stir welds of equal channel angular-pressed aluminium alloys. *Mater. Sci. Eng.*, 354(1-2): 298-305.
- Sefika, K., 2013. Multi-response optimization using the Taguchi-based grey relational analysis: A case study for dissimilar friction stir butt welding of AA6082-T6/AA5754-H111. *Int. J. Adv. Manuf. Tech.*, 68: 795-804.
- Shanmuga Sundaram, N. and N. Murugan, 2010. Tensile behavior of dissimilar friction stir welded joints of aluminium alloys. *Mater. Des.*, 31: 4184-4193.
- Srivatsan, T.S., V. Satish and P. Lisa, 2007. The tensile deformation and fracture behavior of friction stir welded aluminum alloy 2024. *Mater. Sci. Eng.*, 466: 235-245.
- Su, J.Q., T.W. Nelson, R. Mishra and M. Mahoney 2003. Microstructural investigation of friction stir welded 7050-T651 aluminium. *Acta Materialia*, 51(3): 713-729.
- Thomas, W.M., E.D. Nicholas, J.C. Needham, M.G. Murch, P. Templesmith and C.J. Dawes, 1991. Patent. 9125978.8.
- Ying, L., E A. Trillo and L.E. Murr, 2000. Friction-stir welding of aluminum alloy 2024 to silver. *J. Mater. Sci. Lett.*, 19: 1047-1051.
- Zhang, H.W., Z. Zhang and J.T. Chen, 2005. The finite element simulation of the friction stir welding process. *Metall. Mater. Trans. A*, 403: 305-316.